

Tropospheric and stratospheric momentum flux measurements from radar wind data collected at Jicamarca

Dennis M. Riggin*, Erhan Kudeki, Martin Sarango

Colorado Research Associates Division, North West Research Associates, 3380 Mitchell Lane, Boulder, CO 80301, USA

Received 14 January 2003; received in revised form 17 July 2003; accepted 13 October 2003

Abstract

Tropospheric and stratospheric radar wind data obtained at Jicamarca, Perú (11.95°S, 76.87°W) during August 17–26, 1998 have been used to estimate the momentum flux of short-period ($T < 2$ h) wind fluctuations together with the estimation uncertainties. As a result of our study we conclude that momentum flux estimates exceeding the measurement uncertainties can be obtained after about one day of integration.

© 2003 Elsevier Ltd. All rights reserved.

Keywords: Momentum flux; Winds; Radar; Error; Troposphere; Stratosphere

1. Introduction

This paper describes an effort to measure the momentum flux associated with tropospheric and stratospheric wind fluctuations using radar wind data collected by the 50 MHz radar at Jicamarca Radio Observatory (11.95°S, 76.87°W) located near Lima, Perú. Wind measurements were collected at Jicamarca during August 17–26, 1998 using a four beam radar configuration that allowed the estimation of the u , v , and w vector components of the winds with 1-min time resolution. More details on the measurement campaign are given in Riggin et al. (2002). The u , v , and w data were high-pass filtered and subsequently processed to estimate the momentum fluxes (per unit mass) $\langle uw \rangle$ and $\langle vw \rangle$ and their estimation errors. The study was motivated by recent papers by Kudeki and Franke (1998) and Thorsen et al. (2000), concerning statistical errors in radar momentum flux estimation. The goal of the experiment was to conduct a careful error analysis and test whether momentum flux estimates could be obtained that exceed the error bars.

This paper deals with two categories of error that we will refer to as instrumental error and geophysical error. The instrumental error can be described as the total error due to

defects in the measurement. In contrast, geophysical error is present for a perfect anemometer, and can be described as the statistical uncertainty in characterizing a distribution of values with a finite averaging time. Hasebe et al. (1997) uses the term “observational errors” for these uncertainties, while Kudeki and Franke (1998) refers to them as “measurement errors.” This source of noise comes largely from the waves themselves, and can be described as fluctuations which are not representative of the actual gravity wave field that one is attempting to quantify over the averaging period. The error bars that we will estimate will include the combined effects of both instrumental errors and geophysical noise.

The wind and momentum flux estimators used in this study and the details of our error analysis procedure are described in Section 2. The experimental results, including the estimated momentum flux altitude profiles, are presented in Section 3. Finally, Section 4 discusses the results.

2. Momentum flux estimator and its variance

The Jicamarca radar momentum flux estimates are derived from radial velocity data obtained with narrow radar beams pointed $\theta \approx 2.5^\circ$ off-zenith in the east, west, north, and south directions, respectively. Let \tilde{r}'_{n+} and \tilde{r}'_{n-} , $n \in [0, N - 1]$, denote one-minute resolution radial

* Corresponding author.

E-mail address: riggin@colorado-research.com (D.M. Riggin).

velocity estimates extracted from two coplanar Jicamarca radar beams (e.g., east and west pointed). These radial velocity estimates were obtained by fitting the logarithm of one-minute integrated Doppler spectra of the east and west beam signal returns with frequency-shifted generalized-Gaussian functions. Radial velocity estimates obtained with this procedure will in general contain zero-mean errors, $\delta r'_{n\pm}$, due to statistical fluctuations of the spectral data fitted to the generalized-Gaussian model. Thus,

$$\tilde{r}'_{n\pm} \equiv r'_{n\pm} + \delta r'_{n\pm},$$

where $\delta r'_{n\pm}$ will be referred to as instrumental error or instrumental noise from hereon. Estimates of the rms values of $\delta r'_{n\pm}$ were obtained as a by-product of the spectral fitting procedure.

Using the radial velocity data $\tilde{r}'_{n\pm}$, $n \in [0, N-1]$, from an east–west beam pair, unbiased estimates of the wind momentum flux (per unit mass) $\langle uw \rangle$ can be obtained by using the estimator

$$\tilde{C} \equiv \frac{1}{N} \sum_{n=0}^{N-1} \frac{\tilde{r}'_{n+}^2 - \tilde{r}'_{n-}^2}{2 \sin 2\theta} \quad (1)$$

(e.g., Vincent and Reid, 1983), provided that the instrumental error variances $\langle \delta r_{n+}^2 \rangle$ and $\langle \delta r_{n-}^2 \rangle$ are equal (e.g., Worthington and Thomas, 1996) and also provided that the fluctuations in u and w have stationary and horizontally homogeneous statistics. In practice, the summation over n in Eq. (1) represents a summation over time. The same momentum flux estimator (1) can also be written as

$$\tilde{C} = \frac{1}{N} \sum_{n=0}^{N-1} \tilde{u}_n \tilde{w}_n \quad (2)$$

with

$$\tilde{u}_n \equiv \frac{\tilde{r}'_{n+} - \tilde{r}'_{n-}}{2 \sin \theta} \quad (3)$$

and

$$\tilde{w}_n \equiv \frac{\tilde{r}'_{n+} + \tilde{r}'_{n-}}{2 \cos \theta}, \quad (4)$$

denoting the standard estimators for wind components u and w used with dual beam radar data.

Since the momentum flux estimator (2) is unbiased, $\langle \tilde{C} \rangle = C$, and, consequently the estimator variance is

$$\delta C^2 \equiv \langle (\tilde{C} - \langle \tilde{C} \rangle)^2 \rangle = \langle (\tilde{C} - C)^2 \rangle = \langle \tilde{C}^2 \rangle - C^2. \quad (5)$$

Using (2) it follows that

$$\delta C^2 = \frac{1}{N^2} \sum_{n=0}^{N-1} \sum_{m=0}^{N-1} \langle \tilde{u}_n \tilde{w}_n \tilde{u}_m \tilde{w}_m \rangle - C^2. \quad (6)$$

To expand the first term on the right-hand side of Eq. (6) we use the identity $\langle abcd \rangle = \langle ab \rangle \langle cd \rangle + \langle ac \rangle \langle bd \rangle + \langle ad \rangle \langle bc \rangle$ which is valid for all zero-mean Gaussian random variables a , b , c , and d (e.g., Helstrom, 1991). Thus, assuming that

\tilde{u}_n and \tilde{w}_n are zero-mean Gaussian random variables,

$$\begin{aligned} \langle \tilde{u}_n \tilde{w}_n \tilde{u}_m \tilde{w}_m \rangle &= \langle \tilde{u}_n \tilde{w}_n \rangle \langle \tilde{u}_m \tilde{w}_m \rangle + \langle \tilde{u}_n \tilde{u}_m \rangle \langle \tilde{w}_n \tilde{w}_m \rangle \\ &\quad + \langle \tilde{u}_n \tilde{w}_m \rangle \langle \tilde{w}_n \tilde{u}_m \rangle \end{aligned} \quad (7)$$

in which case

$$\delta C^2 = \frac{1}{N^2} \sum_{n=0}^{N-1} \sum_{m=0}^{N-1} \{ \langle \tilde{u}_n \tilde{u}_m \rangle \langle \tilde{w}_n \tilde{w}_m \rangle + \langle \tilde{u}_n \tilde{w}_m \rangle \langle \tilde{w}_n \tilde{u}_m \rangle \}, \quad (8)$$

since $\langle \tilde{u}_n \tilde{w}_n \rangle \langle \tilde{u}_m \tilde{w}_m \rangle = \langle uw \rangle^2 = C^2$. Finally, since stationarity has been assumed, $\langle \tilde{u}_n \tilde{u}_m \rangle \equiv R_{\tilde{u}}(m-n)$, $\langle \tilde{w}_n \tilde{w}_m \rangle \equiv R_{\tilde{w}}(m-n)$, and $\langle \tilde{u}_n \tilde{w}_m \rangle \equiv R_{\tilde{u}\tilde{w}}(m-n)$, and therefore (Oppenheim et al., 1999), for $p = m - n$,

$$\begin{aligned} \delta C^2 &= \frac{1}{N} \sum_{p=-(N-1)}^{N-1} \left(1 - \frac{|p|}{N} \right) \\ &\quad \times \{ R_{\tilde{u}}(p) R_{\tilde{w}}(p) + R_{\tilde{u}\tilde{w}}(p) R_{\tilde{u}\tilde{w}}(-p) \}. \end{aligned} \quad (9)$$

The variables $R_{\tilde{u}}(p)$ and $R_{\tilde{w}}(p)$ denote the auto-correlation functions (ACF) of random data \tilde{u}_n and \tilde{w}_n while $R_{\tilde{u}\tilde{w}}(p)$ represents the cross-correlation function (XCF) of the same data pairs.

A theoretical study of the bounds of momentum flux error variance δC^2 for the case $\delta r'_{n\pm} = 0$ (i.e., zero instrumental error) was reported in Kudeki and Franke (1998). Thorsen et al. (2000) generalized the results of Kudeki and Franke (1998) to include instrumental noise effects and also examined the dependence of δC^2 on the radar beam angle θ . These studies suggested that unless the data length N is very large, $\delta C^2 \gg C^2$ and that δC^2 is of the order of the first component in Eq. (9) that depends on auto-correlations, $R_{\tilde{u}}(p)$ and $R_{\tilde{w}}(p)$. In view of these results, the $R_{\tilde{u}\tilde{w}}(p)$ -dependent second term in Eq. (9) can be neglected, and the momentum flux variance can be approximated as

$$\delta C^2 \approx \frac{1}{N} \sum_{p=-(N-1)}^{N-1} \left(1 - \frac{|p|}{N} \right) R_{\tilde{u}}(p) R_{\tilde{w}}(p). \quad (10)$$

Finally, if the $R_{\tilde{u}}(p) R_{\tilde{w}}(p)$ product is negligible for all p except $p = 0$,

$$\delta C^2 \approx \frac{R_{\tilde{u}}(0) R_{\tilde{w}}(0)}{N} = \frac{\langle \tilde{u}_n^2 \rangle \langle \tilde{w}_n^2 \rangle}{N} \quad (11)$$

should be a reasonable approximation for the error variance δC^2 .

As shown above, the rms error (δC) in the momentum flux estimates (\tilde{C}) is dependent on the ACF's $R_{\tilde{u}}(p)$ and $R_{\tilde{w}}(p)$ of noisy wind data \tilde{u}_n and \tilde{w}_n . The error (δC) as defined by Eq. (10) accounts for both instrumental and geophysical noise in \tilde{C} , and it is also valid with any type of pre-filtered (e.g., high-pass) \tilde{u}_n and \tilde{w}_n data used in band-limited momentum flux estimation. In the next section we will present examples of estimates of $R_{\tilde{u}}(p)$ and $R_{\tilde{w}}(p)$ as well as \tilde{C} and δC obtained with high-pass filtered Jicamarca wind data from stratospheric and tropospheric heights.

We will close this section by examining the co-variance of momentum flux estimates obtained with wind data from neighbouring radar range gates. Using the notation \tilde{C}_1 and \tilde{C}_2 to refer to estimates from neighbouring range gates, and noting that $\langle \tilde{C}_1 \rangle = C_1$ and $\langle \tilde{C}_2 \rangle = C_2$, we first establish that

$$\delta C_{12}^2 \equiv \langle (\tilde{C}_1 - \langle \tilde{C}_1 \rangle)(\tilde{C}_2 - \langle \tilde{C}_2 \rangle) \rangle \quad (12)$$

Thus, using Eq. (2),

$$\delta C_{12}^2 = \langle \tilde{C}_1 \tilde{C}_2 \rangle - C_1 C_2$$

$$= \frac{1}{N^2} \sum_{n=0}^{N-1} \sum_{m=0}^{N-1} \langle \tilde{u}_n \tilde{w}_n \tilde{u}_m \tilde{w}_m \rangle - C_1 C_2, \quad (13)$$

where indices n and m now refer to samples from adjacent heights. Using Eq. (7) once again, and since $\langle \tilde{u}_n \tilde{w}_n \rangle \langle \tilde{u}_m \tilde{w}_m \rangle = C_1 C_2$ we find that

$$\delta C_{12}^2 \approx \frac{1}{N} \sum_{p=-(N-1)}^{N-1} \left(1 - \frac{|p|}{N} \right) R_{\tilde{u}\tilde{u}'}(p) R_{\tilde{w}\tilde{w}'}(p), \quad (14)$$

where $R_{\tilde{u}\tilde{u}'}(p)$ and $R_{\tilde{w}\tilde{w}'}(p)$ denote the cross-correlation of \tilde{u}_n and \tilde{w}_n data from adjacent range gates. When the covariance δC_{12}^2 is of the order of variance δC^2 , estimation errors in adjacent heights \tilde{C}_1 and \tilde{C}_2 are highly correlated and the height profile of momentum flux may appear smooth despite the presence of potentially large estimation errors. Unless $R_{\tilde{u}\tilde{u}'}(0) \ll R_{\tilde{u}}(0)$ and $R_{\tilde{w}\tilde{w}'}(0) \ll R_{\tilde{w}}(0)$, profile smoothness should not be regarded as a criterion of estimation quality.

3. Experimental results

We used radial velocity data \tilde{r}'_{n+} and \tilde{r}'_{n-} , $n \in [0, N - 1]$, obtained from one-minute averaged Doppler spectra of Jicamarca east and west beam signals to calculate one-minute \tilde{u}_n and \tilde{w}_n estimates according to Eqs. (3) and (4). North and south beam returns were processed likewise to obtain a second set of one-minute \tilde{v}_n and \tilde{w}_n estimates. Note that only the coplanar \tilde{w}_n samples should be combined with the corresponding horizontal samples when estimating momentum flux. Using the same symmetric coplanar beams to form the horizontal and vertical velocities avoids mixing horizontal (u, v) momentum flux terms with the desired vertical flux of horizontal momentum. The estimates were obtained with 450 m height resolution starting at 8 km altitude, provided by a 16-baud complementary coded transmitter pulses with 3 μ s baud length. The data collection was nearly continuous over a 10-day period of August 17–26, 1998.

Prior to momentum flux estimation using Eq. (2) we high-pass filtered the data fields \tilde{u}_n and \tilde{w}_n from the east/west beam pair and \tilde{v}_n and \tilde{w}_n from north/south beam pair to suppress the wind components with periods larger than 2 h. This was accomplished by subtracting a low-pass response of the data obtained with a running-mean raised cosine filter function from the original data set. Missing data points were ignored when computing the running mean average.

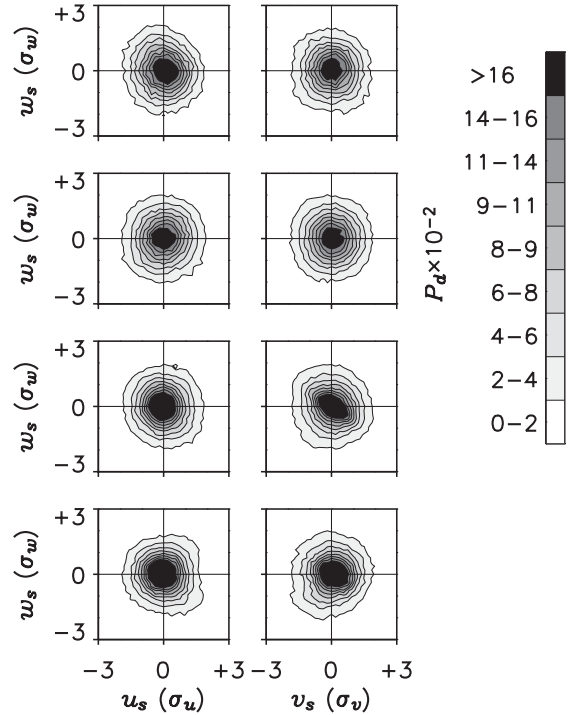


Fig. 1. Probability distribution plots of high-pass filtered probability densities of \tilde{u}_n versus \tilde{w}_n (left-hand side) and \tilde{v}_n vs. \tilde{w}_n (right-hand side). Data for four consecutive height intervals, each containing ~ 10 range gates.

The filter suppressed the 2 h period component of the wind data by 50%. Before computing probability distribution functions (PDF's) of the wind fluctuations, the variables were divided by their respective standard deviation at each height. Fig. 1 shows contour plots depicting the PDF's of high-passed and standardized (unit standard deviation) \tilde{u}_n and \tilde{w}_n (as well as \tilde{v}_n and \tilde{w}_n) data averaged in four height intervals (8.45–12.05 km, 12.5–16.55 km, 17–21.05 km, and 21.5–25.55 km). Each of the distributions is an average of ~ 10 heights and all 10 days. The distributions are bell-like with weak co-variances $\langle \tilde{u}_n \tilde{w}_n \rangle$ (and $\langle \tilde{v}_n \tilde{w}_n \rangle$). The units of the PDF's are such that their integrals over the domain equals one.

Fig. 2 depicts examples of the ACF's, $R_{\tilde{u}}(p)$ and $R_{\tilde{w}}(p)$, obtained from \tilde{u}_n and \tilde{w}_n data using the estimators

$$\tilde{R}_{\tilde{u}}(p) = \frac{1}{K} \sum_{n=0}^{K-1} \tilde{u}_n \tilde{u}_{n+p} \quad (15)$$

and

$$\tilde{R}_{\tilde{w}}(p) = \frac{1}{K} \sum_{n=0}^{K-1} \tilde{w}_n \tilde{w}_{n+p}. \quad (16)$$

In Eqs. (15) and (16), K is the length of the subsets of \tilde{u}_n and \tilde{w}_n data used for ACF estimation, where K is selected

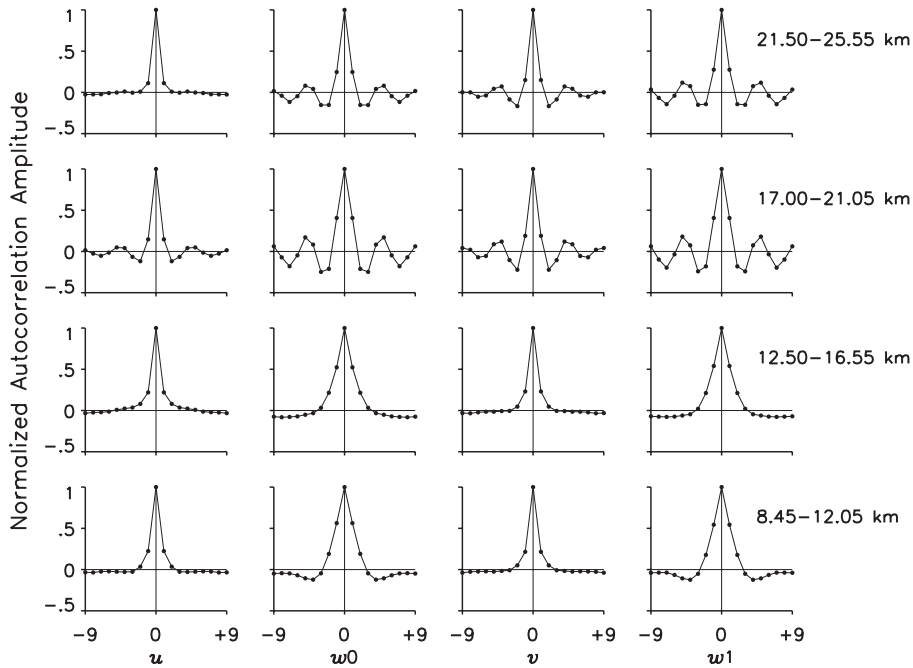


Fig. 2. ACF's of \tilde{u}_n and \tilde{w}_n as well as \tilde{v}_n and \tilde{w}_n data estimated for the same height intervals used in Fig. 1 and using the entire 10 days of measurements. The individual ACF's were self-normalized by their zero-lag values and the labels w_0 and w_1 refer to \tilde{w}_n data obtained from east–west and north–south beam pairs, respectively.

to satisfy $K \ll N$. Note that the $R_{\tilde{u}}(p)$ (as well as the $R_{\tilde{v}}(p)$) estimates are generally small for p other than 0, indicating that Eq. (10) should be well approximated by Eq. (11). The ACF's are plotted for the same heights as the PDF's in Fig. 1.

Fig. 3(a) and (c) show profiles of campaign-averaged meridional and zonal momentum fluxes calculated using Eq. (2) and its meridional counterpart. A circle, arbitrarily drawn in Fig. 1 of diameter 2.5 in standard deviation units would lie outside all the PDF contours. Panels 3(b) and (d) show the impact of excluding the “tail” samples that lie outside this 2.5 standard deviation circle. The sign of the momentum flux is generally the same after excluding the “tails”, but the magnitude is considerably smaller. Thus, much of the momentum flux signal resides in the distribution tails, even though the tails only comprise $\sim 10\%$ of the samples. The error envelope (shaded area) was calculated from Eq. (10). The error envelope drawn is actually $\pm 2\delta C$ (total width of $4\delta C$) to correspond to the 95% confidence interval for a Gaussian distribution. The error bars were calculated from Eq. (11). These are reasonable approximations to the error envelope, but of course are smaller since they assume that the samples are completely statistically independent. The approximation of Eq. (11) is not as good for panels 3(c) and (d), implying that samples in the central part of the distributions of Fig. 1 are more correlated from sample-to-sample than those in the tails of the distributions.

4. Discussion

The experimental results shown in Section 3 suggest that tropospheric and stratospheric momentum flux estimation at Jicamarca is possible when $\tilde{u}_n \tilde{w}_n$ products of high-pass filtered wind data \tilde{u}_n and \tilde{w}_n obtained with one-minute time resolution are averaged over at least a few days of observations. It appears that the uncertainty in momentum flux estimates is reduced by the square root of the number of terms averaged, implying that the noise in individual $\tilde{u}_n \tilde{w}_n$ terms are nearly independent from one minute to the next. A contributing factor to the rapid decorrelation of the horizontal wind is the presence of large instrumental noise component in \tilde{u}_n that has been propagated from relatively small instrumental errors $\delta r'_{n\pm}$ included in $\tilde{r}'_{n\pm}$. Using Eq. (3) and applying straightforward error analysis it can be seen that the rms instrumental error in \tilde{u}_n is

$$\delta u_{\text{inst}} = \frac{\sqrt{\langle \delta r_{n+}'^2 \rangle + \langle \delta r_{n-}'^2 \rangle}}{2 \sin \theta}, \quad (17)$$

which is large compared to rms instrumental error in \tilde{w}_n ,

$$\delta w_{\text{inst}} = \frac{\sqrt{\langle \delta r_{n+}'^2 \rangle + \langle \delta r_{n-}'^2 \rangle}}{2 \cos \theta} \quad (18)$$

because of the small denominator in Eq. (17) compared with Eq. (18). When instrumental noise in \tilde{u}_n dominates

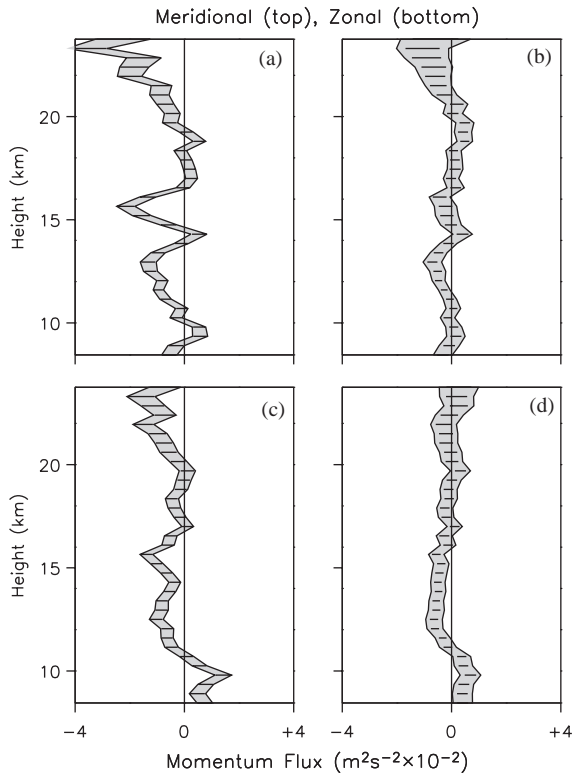


Fig. 3. Momentum flux profiles and error bars computed from 10-day averages for (a) meridional component; (c) zonal component. Profiles (b) and (d) correspond to profiles (a) and (c), respectively, except that they were calculated after the removal of wind pair data in the fringes of the distributions shown in Fig. 1 (no rms wind speed fluctuations exceeding 2.5 in standard deviation units). The error envelope (shaded area) is $\pm\delta C$, with δC as calculated from Eq. (10), while the error bars were calculated from Eq. (11).

over geophysical noise (e.g., variations in u due to a superposition of wave effects), errors in \tilde{u}_n are by and large uncorrelated between the 1-min estimates (since instrumental errors are independent from one spectral fit to the next) and therefore the precision of momentum flux estimates improves as $\sqrt{1/N}$.

The large instrumental noise in \tilde{u}_n also helps to explain the shape of the \tilde{u}_n ACF's $\tilde{R}_{\tilde{u}}(p)$ shown in Fig. 2. Note how $\tilde{R}_{\tilde{u}}(p)$ drops rapidly with increasing p as compared to $\tilde{R}_{\tilde{v}}(p)$. This behavior indicates the presence of a “white noise spike” in $\tilde{R}_{\tilde{u}}(p)$ at the “zero lag” $p = 0$, which is exactly what would be expected if \tilde{u}_n were strongly contaminated by instrumental noise. However, the ACF's of the horizontal wind components appear to be compact compared with the vertical wind components even at the larger lags. One possible interpretation is that wind fluctuations correspond to vertically aligned convective motions, rather than propagating waves. Riggin et al. (2002) showed evidence for strong convective (up–down) motions in the troposphere which

terminated in the vicinity of the tropopause (~ 16 km) in an analysis of the lower-frequency winds during the same August 1998 campaign.

It is interesting to note here the impact of instrumental as well as geophysical noise on possible biases that can arise in wind variance and momentum flux estimation. First, we observe that high-pass filtered \tilde{u}_n data will be a sum of u fluctuations in the frequency band of interest (the only part of \tilde{u}_n that we really want), instrumental noise, and so called fluctuation induced errors (e.g., Kudeki et al., 1993) arising from the inhomogeneity of wind vectors within the two radar beams. Consequently, the variance $\langle \tilde{u}_n^2 \rangle$ of \tilde{u}_n is biased from the variance $\langle u^2 \rangle$ of u by the sum of the variances due to instrumental noise- and fluctuation-induced errors. The variances will generally be overestimated. However, if two conditions are met, the covariance $\langle \tilde{u}_n \tilde{w}_n \rangle$ of filtered \tilde{u}_n and \tilde{w}_n data will be unbiased and equal to the wind momentum flux (per unit mass) $\langle uw \rangle$ in the frequency band of interest despite the presence of instrumental and other errors in \tilde{u}_n and \tilde{w}_n data. As already pointed out in Section 2, one of these conditions is to have equal rms levels of instrumental noise in the \tilde{r}'_{n+} and \tilde{r}'_{n-} data. The second condition is stationarity and horizontal homogeneity of the wind fluctuations probed by the radar. When both conditions are met, the total error variances in \tilde{r}'_{n+} and \tilde{r}'_{n-} become equal and cancel out exactly in the numerator of the expected value of the momentum flux estimator (1). This cancellation occurs whether the joint distributions of \tilde{u}_n and \tilde{w}_n fluctuations have Gaussian forms or not. This remarkable fact, i.e., the immunity of $\langle \tilde{u}_n \tilde{w}_n \rangle$ and $\langle \tilde{v}_n \tilde{w}_n \rangle$ from fluctuation-induced biases that contaminate $\langle \tilde{u}_n^2 \rangle$, $\langle \tilde{v}_n^2 \rangle$ and $\langle \tilde{w}_n^2 \rangle$ is one reason why it is possible to obtain meaningful radar momentum flux estimates with sufficiently long integrations.

Fig. 4 shows daily averaged momentum flux profiles. The most striking feature in the profiles is a negative peak in the meridional flux at ~ 15 km during August 21–22, and 24–25. This feature is consistent with the elongation of the contours seen in Fig. 1. Note in particular the second panel from the bottom on the right-hand side of Fig. 1. The negative slope of the elongated region in this panel demonstrate that we are measuring a true momentum flux due to a negative correlation between v and w . The southward momentum flux features are repeatable from day-to-day, but it is not possible to tell from the net momentum profiles whether the peaks are due to excitation of southward propagating waves at this height or a weakening (e.g., due to dissipation) of the northward propagating waves.

The characteristics of this momentum flux peak can be investigated by segregating the momentum flux into positive and negative momentum flux contributions as shown in Fig. 5. The positive momentum flux contribution is (in the zonal case) the average of all the positive uw products (samples for which u and w are both positive or both negative). The negative momentum flux component, shown as a dashed line is the summation of all the negative uw products. The absolute value of the negative momentum flux

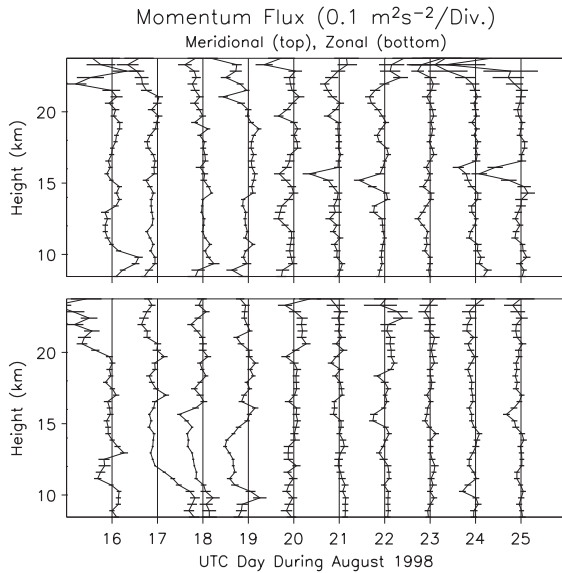


Fig. 4. Vertical profiles of daily averaged meridional momentum flux (top), and zonal momentum flux (bottom). The profiles are offset by $0.1 \text{ m}^2 \text{ s}^{-2}$. The error bars were calculated from Eq. (11).

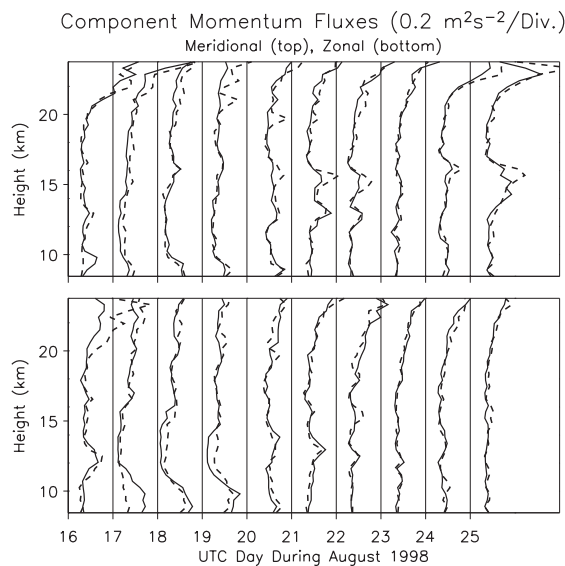


Fig. 5. Vertical profiles of daily averaged positive and negative momentum flux components. The upper panel is meridional and the lower panel zonal. The positive momentum flux component, shown as solid lines is the average of all the horizontal/vertical wind products that are positive. The negative zonal momentum flux component, shown as dashed lines is the average of all negative horizontal/vertical wind products, then taking the absolute value of the average. The profiles are offset by $0.2 \text{ m}^2 \text{ s}^{-2}$.

contribution has been taken so that it can be easily compared with the positive momentum flux contribution. The lower panel of Fig. 5 shows the positive (solid line) and

negative (dashed line) contributions to the total zonal momentum flux and the upper panel shows the same for the meridional momentum flux. The positive and negative contributions are larger in magnitude than the total momentum flux, so the profiles in Fig. 5 are offset by $0.2 \text{ m}^2 \text{ s}^{-2}$, compared with $0.1 \text{ m}^2 \text{ s}^{-2}$ offsets in Fig. 4. Fig. 5 shows that the positive and negative momentum flux contributions tend to track each other. Careful comparison of Fig. 4 with Fig. 5 shows that the southward momentum flux peaks seen in Fig. 4 are associated with *northward*, as well as southward peaks in the component momentum fluxes. One possible interpretation is that these peaks correspond to turbulent motions, rather than propagating waves. Riggin et al. (2002) showed evidence for strong convective (up–down) motions in the troposphere during the August 1998 campaign that terminated in the vicinity of the tropopause ($\sim 16 \text{ km}$). Enhanced turbulence might be expected at this height where vertical motions are impeded due to the enhanced stability.

5. Conclusions

In this work we have shown that the four beam configuration at Jicamarca is suitable for high-frequency momentum flux estimation in the troposphere and lower stratosphere provided that several days of continuous measurements are available. In view of the large instrument noise involved in horizontal wind estimation momentum flux error bars vary as $N^{-1/2}$, where N denotes the number of available radial wind estimates from dual co-planar beams. The availability of continuous wind estimates (in height and time) at tropospheric and stratospheric heights helps with compiling the required statistics after only a few days of observations.

Future studies should consider the impact of the violation of wind fluctuation stationarity on momentum flux estimates. The stationarity assumption is likely to be violated during integration periods approaching or exceeding a day, and, as a result, statistically significant flux estimates must represent a temporal average of time-dependent momentum flux variations. There is evidence of this in the day-to-day variability of the flux profiles shown in Fig. 4. Potential biases arising from episodic violations of horizontal homogeneity and/or balanced instrumental noise assumptions during extended integration periods should be considered and assessed.

The net momentum flux after long (e.g., 10 day) averages was found to be generally weak, and at some heights nearly indistinguishable from zero. In these cases the sign of the net momentum flux is indeterminate, although the underlying PDF can be determined quite accurately. Our earlier assumptions concerning the Gaussian character of the distributions were necessary for developing a tractable formula for the error variance δC^2 . However, the distribution function widths and shapes might provide more useful information than the momentum flux as a single number. Particular attention should be given to the distribution tails, since these few samples make a relatively large contribution to the net

momentum flux. We plan to examine the distributions in more detail in future studies.

Acknowledgements

The help provided by the staff and engineers of Jicamarca Radio Observatory is gratefully acknowledged. The Observatory is operated by the Geophysical Institute of Perú, Ministry of Education, with support from the National Science Foundation of the United States. This research is supported by the Division of Atmospheric Sciences of the National Science Foundation through Grants ATM-9709030 at CoRA and ATM-9709251 at the University of Illinois.

References

- Hasebe, F., Tsuda, T., Nakamura, T., Burrage, M.D., 1997. Validation of HRDI MLT winds with meteor radars. *Annals of Geophysics* 15, 1142–1157.
- Helstrom, C.W., 1991. *Probability and Stochastic Processes for Engineers*, 2nd Edition. Macmillan, New York.
- Kudeki, E., Rastogi, P.K., Sürücü, F., 1993. Systematics errors in radar wind estimation: Implications for comparative measurements. *Radio Science* 28, 169–179.
- Kudeki, E., Franke, S.J., 1998. Statistics of momentum flux estimation. *Journal of Atmospheric and Solar-Terrestrial Physics* 60, 1549–1553.
- Oppenheim, A.V., Schafer, R.W., Buck, J.R., 1999. *Discrete-Time Signal Processing*, 2nd Edition. Prentice-Hall, Upper Saddle River, NJ.
- Riggin, D.M., Kudeki, E., Feng, Z., Sarango, M.F., Lieberman, R.S., 2002. Jicamarca Radar observations of the diurnal and semidiurnal tide in the troposphere and lower stratosphere. *Journal of Geophysical Research* 107 (8), 4062. DOI 10.1029/2001JD001216.
- Thorsen, D., Franke, S.J., Kudeki, E., 2000. Statistics of momentum flux estimation using the dual coplanar beam technique. *Geophysical Research Letters* 103, 3193–3196.
- Vincent, R.A., Reid, I.M., 1983. HF Doppler measurements of mesospheric gravity wave momentum fluxes. *Journal of Atmospheric Science* 40, 1321–1333.
- Worthington, R.M., Thomas, L., 1996. The measurement of gravity-wave momentum flux in the lower atmosphere using VHF radar. *Radio Science* 31, 1501–1517.